Enhanced hydrogen storage properties of MgH2 co-catalyzed with K2NiF6 and CNTs

2 authors, including:

Mohammad Ismail
Universiti Malaysia Terengganu

40 PUBLICATIONS **590** CITATIONS

Dalton Transactions

PAPER

Enhanced hydrogen storage properties of MgH$_2$ co-catalyzed with K$_2$NiF$_6$ and CNTs

N. N. Sulaiman and M. Ismail*

The composite of MgH$_2$/K$_2$NiF$_6$/carbon nanotubes (CNTs) is prepared by ball milling, and its hydrogenation properties are studied for the first time. MgH$_2$ co-catalyzed with K$_2$NiF$_6$ and CNTs exhibited an improvement in the onset dehydrogenation temperature and isothermal de/rehydrogenation kinetics compared with the MgH$_2$–K$_2$NiF$_6$ composite. The onset dehydrogenation temperature of MgH$_2$ doped with 10 wt% K$_2$NiF$_6$ and 5 wt% CNTs is 245 °C, which demonstrated a reduction of 25 °C compared with the MgH$_2$ + 10 wt% K$_2$NiF$_6$ composite. In terms of rehydrogenation kinetics, MgH$_2$ doped with 10 wt% K$_2$NiF$_6$ and 5 wt% CNTs samples absorbed 3.4 wt% of hydrogen in 1 min at 320 °C, whereas the MgH$_2$ + 10 wt% K$_2$NiF$_6$ sample absorbed 2.6 wt% of hydrogen under the same conditions. For dehydrogenation kinetics at 320 °C, the MgH$_2$ + 10 wt% K$_2$NiF$_6$ + 5 wt% CNTs sample released 3.3 wt% hydrogen after 5 min of dehydrogenation. By contrast, MgH$_2$ doped with 10 wt% K$_2$NiF$_6$ released 3.0 wt% hydrogen in the same time period. The apparent activation energy, E_a, for the dehydrogenation of MgH$_2$ doped with 10 wt% K$_2$NiF$_6$ reduced from 100.0 kJ mol^{-1} to 70.0 kJ mol^{-1} after MgH$_2$ was co-doped with 10 wt% K$_2$NiF$_6$ and 5 wt% CNTs. Based on the experimental results, the hydrogen storage properties of the MgH$_2$/K$_2$NiF$_6$/CNTs composite is enhanced because of the catalytic effects of the active species of KF, KH and Mg$_2$Ni that are formed *in situ* during dehydrogenation, as well as the unique structure of CNTs.

1. Introduction

Hydrogen is an attractive potential energy carrier for energy applications mainly because of its low pollution factor.[1] Despite the fact that hydrogen is an ideal candidate for energy carriers, concerns surrounding the storage of hydrogen are a major issue. Currently, hydrogen can be stored in a gaseous form, liquid form (as a cryogenic liquid) and solid form (absorbed gas in solid material).[2] The commercialisation of hydrogen storage in pressurised gas and cryogenic liquid forms have faced two major technical challenges, namely, safety and cost. Thus, solid-state hydrogen storage is an attractive option as it has high gravimetric hydrogen capacity and favourable safety considerations.[3]

At present, there are two categories of hydrogen storage in solid-state materials, which are chemically bound hydrogen (such as metal hydrides and complex hydrides) and physically bound hydrogen (such as carbon materials and metal–organic frameworks). Among them, magnesium hydride (MgH$_2$) is considered one of the most promising materials for solid-state hydrogen storage because of its high hydrogen storage capacity

(>6 wt%). MgH$_2$ also has the advantages of low cost and superior reversibility. However, high thermodynamic stability ($\Delta H = -75$ kJ mol^{-1} H$_2$) and slow sorption kinetics render MgH$_2$ impractical for solid-state hydrogen storage.[4] Thus, to overcome these disadvantages, many studies have investigated several techniques for improving its sorption kinetics and lowering the thermodynamic stability. These techniques include reducing the grain size through ball milling,[5] doping with catalyst,[6–9] using a destabilizing concept (reacting with other metals or metal hydrides),[10,11] and a ball-milling process assisted by dielectric-barrier discharge plasma for dual-tuning the thermodynamics and kinetics.[12–16] Currently, doping MgH$_2$ with a catalyst by the ball milling method has been the focus of intensive research. Catalysis doping can be divided into several categories such as using metals,[17] hydrogen storage alloys,[18] metal halides,[19–22] metal oxides, and a carbon-based catalyst.[23,24]

Previous studies have reported the positive effects of carbon nanotubes (CNTs) towards the improvement of the hydrogen storage properties of MgH$_2$.[25,26] The combination of metals or metal halides/oxides with CNTs as mixed dopants has attracted the attention of many researchers with several studies conducted for the MgH$_2$/co-catalyst system.[27–33] The synergistic interaction among metals or metal halides/oxides and CNTs is an effective approach to improve the hydrogen storage properties of MgH$_2$.

School of Ocean Engineering, Universiti Malaysia Terengganu, 21030 Kuala Terengganu, Malaysia. E-mail: mohammadismail@umt.edu.my; Fax: +609-6683991; Tel: +609-6683487

Recently, we found that K_2NiF_6 enhances the hydrogen sorption properties of MgH_2.[34] Based on the encouraging results of the MgH_2–K_2NiF_6 composite, the study of the effect of the K_2NiF_6–CNTs composite as a co-catalyst for the sorption behaviour of MgH_2 may yield interesting findings. In the present study, we hypothesised that the hydrogen storage properties could be enhanced by MgH_2 co-catalyzed with K_2NiF_6 and CNTs. The improvement of the hydrogenation of MgH_2 co-doped with K_2NiF_6 and CNTs is due to the combination of the three interesting elements (*i.e.*, K, Ni and F species) with the catalytic effect of CNTs. To date, no studies have reported the effects of MgH_2 co-doped with K_2NiF_6 and CNTs on the hydrogenation performance of MgH_2 for solid-state hydrogen storage. Thus, this paper proposes to investigate the effects of CNTs as a co-dopant on the hydrogen sorption properties of the MgH_2/K_2NiF_6 composite. The hydrogen storage properties and reaction mechanism of the MgH_2/K_2NiF_6/CNTs composite were investigated using a pressure-composition-temperature (PCT) study, differential scanning calorimetry (DSC), X-ray diffraction (XRD) and scanning electron microscopy (SEM). The possible catalytic mechanism from the results obtained is discussed further in this paper.

2. Experimental section

All the materials used, namely, pure MgH_2 (hydrogen storage grade, 98% purity), K_2NiF_6 (99% purity) and multi walled carbon nanotubes (MWCNTs) (>90% carbon basis, diameter = 110–170 nm, length = 5–9 μm) were purchased from Sigma Aldrich. For simplicity, MWCNTs will be referred to as CNTs. The materials were used as received with no further purification or pretreatment. To eliminate the influence of oxygen and moisture, all the samples were handled in an MBraun Unilab glove box under an argon atmosphere. 10 wt% K_2NiF_6 and 5 wt%/10 wt% CNTs were mixed with 150 mg of MgH_2. Pure MgH_2 and MgH_2 + 10 wt% K_2NiF_6 were also prepared under the same conditions for comparison purpose. All the samples used were milled for 1 h at 400 rpm in a planetary ball mill (NQM-0.4). The samples were loaded into a sealed stainless steel vial, together with four hardened stainless steel balls. The ratio of the weight of the balls to the weight of the powder was 40 : 1.

The temperature-programmed-desorption (TPD) and the de/rehydrogenation kinetics experiments were performed in Sieverts-type pressure-composition temperature (PCT) apparatus (Advanced Material Corporation). About 100 mg of the sample was loaded into a sample vessel in the glove box. For the TPD experiment, all the samples were heated in a vacuum chamber and the amount of desorbed hydrogen was measured to determine the lowest decomposition temperature. The heating rate for the TPD experiment was 5 °C min^{-1} and the samples were heated from 25 °C to 450 °C. The de/rehydrogenation kinetics measurements were conducted at the desired temperature with the initial hydrogen pressure of 33 atm and 1.0 atm, respectively. The hydrogen capacity was expressed in weight percentage (wt%).

X-ray diffraction (XRD) (Rigaku MiniFlex II diffractometer with Cu Kα radiation) was used to study the reaction pathway of the samples. In this study, we used XRD to identify what kind of chemical compound existed in the samples before and after desorption as well as absorption. θ–2θ scans were carried out over diffraction angles from 20° to 80° with a speed of 2.00° min^{-1}. All the sample preparation was done in a glove box to prevent the occurrence of oxidation of the sample. Before measurement, a small amount of sample was spread uniformly on the sample holder, covered with tape and then sealed in plastic wrap to minimize exposure to air during the measurement.

DSC analysis of the dehydrogenation process was carried out on a Mettler Toledo TGA/DSC. The sample of about 5–10 mg was loaded into an alumina crucible, then was put into a sealed glass bottle to prevent the sample from oxidation during transportation from the glove box to the TGA/DSC instrument. A reference material of an empty alumina crucible was used in the analysis. The different heating rates were applied with a 50 ml min^{-1} gas flow when the samples were heated from 25 °C to 500 °C under an argon atmosphere.

Scanning electron microscopy (SEM; JEOL JSM-6360LA) was used to investigate the morphology of the samples. The samples were prepared on a carbon tape and then coated with ultrathin gold spray under vacuum by using vacuum sputter coating. These samples were also prepared in the glove box in order to minimize the oxidation.

3. Results and discussion

The dehydrogenation behaviour of as-received MgH_2, as-milled MgH_2, MgH_2 + 10 wt% K_2NiF_6, MgH_2 + 10 wt% K_2NiF_6 + 5 wt% CNTs and the MgH_2 + 10 wt% K_2NiF_6 + 10 wt% CNTs composite was investigated by using TPD, as shown in Fig. 1. The
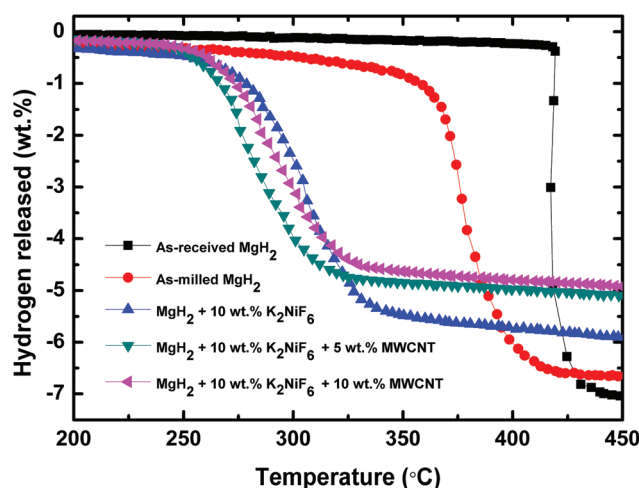
Fig. 1 TPD curves for the dehydrogenation of as-received MgH_2, as-milled MgH_2, MgH_2 + 10 wt% K_2NiF_6, MgH_2 + 10 wt% K_2NiF_6 + 5 wt% CNTs and MgH_2 + 10 wt% K_2NiF_6 + 10 wt% CNTs.

as-received MgH$_2$ started to release hydrogen at about 417 °C, with a total dehydrogenation capacity of 7.1 wt% H$_2$ at 450 °C. Meanwhile, the onset dehydrogenation temperature of MgH$_2$ slightly reduced to about 355 °C after milling, with total hydrogen desorption of 6.7 wt%. This result showed that the milling process also affected the onset desorption temperature of MgH$_2$. After MgH$_2$ was doped with 10 wt% K$_2$NiF$_6$, the onset decomposition temperature of MgH$_2$ was greatly enhanced. The dehydrogenation temperature of MgH$_2$ + 10 wt% K$_2$NiF$_6$ decreased to about 270 °C, which was lower by 147 °C and 85 °C compared with that of as-received and as-milled MgH$_2$, but the amount of hydrogen released decreased to 5.9 wt%. Furthermore, MgH$_2$ + 10 wt% K$_2$NiF$_6$ + 5 wt% CNTs and MgH$_2$ + 10 wt% K$_2$NiF$_6$ + 10 wt% CNTs had a positive effect on the onset dehydrogenation temperature of MgH$_2$. The desorption of the 10 wt% K$_2$NiF$_6$ + 5 wt% CNTs co-doped MgH$_2$ sample started at around 245 °C with a total dehydrogenation capacity of 5.1 wt%, which was a reduction of about 172 °C, 110 °C and 25 °C compared with as-received MgH$_2$, as-milled MgH$_2$ and MgH$_2$ + 10 wt% K$_2$NiF$_6$, respectively. The results of MgH$_2$ + 10 wt% K$_2$NiF$_6$ + 10 wt% CNTs are also included in the graph for comparison. The sample started to release hydrogen at about 251 °C with a total hydrogen release capacity of 5.0 wt% H$_2$, which is almost the same as the hydrogen dehydrogenation capacity of MgH$_2$ + 10 wt% K$_2$NiF$_6$ + 5 wt% CNTs. It can be seen clearly that the onset dehydrogenation temperature of MgH$_2$ + 10 wt% K$_2$NiF$_6$ + 5 wt% CNTs was lower than MgH$_2$ + 10 wt% K$_2$NiF$_6$ + 10 wt% CNTs. This correlated with our previous study which reported that this finding may be due to the excessive catalytic effects brought about by the relatively high levels of the added catalyst.[22,35] In addition, Barkhordarian et al.[36] also reported the same phenomenon in their paper. They claimed that only 0.5 mol% Nb$_2$O$_5$ was enough to give the fastest kinetics with a 7.0 wt% total dehydrogenation capacity. All the results indicated that K$_2$NiF$_6$ and CNTs demonstrated synergetic effects as a mixed dopant.

Fig. 2(a) presents the isothermal rehydrogenation kinetics curve for as-milled MgH$_2$, MgH$_2$ + 10 wt% K$_2$NiF$_6$, MgH$_2$ + 10 wt% K$_2$NiF$_6$ + 5 wt% CNTs, and the MgH$_2$ + 10 wt% K$_2$NiF$_6$ + 10 wt% CNTs composite measured at a constant temperature of 320 °C under 33.0 atm of H$_2$. The results suggested that MgH$_2$ + 10 wt% K$_2$NiF$_6$ + 5 wt% CNTs had the fastest kinetics rate compared with the others. Moreover, the K$_2$NiF$_6$ and CNTs co-doped MgH$_2$ samples showed better hydrogen absorption properties than the as-milled MgH$_2$ and the MgH$_2$ + 10 wt% K$_2$NiF$_6$ composite. The sample of MgH$_2$ doped with 10 wt% K$_2$NiF$_6$ absorbed 2.6 wt% of H$_2$ in 1 min, whereas the as-milled MgH$_2$ absorbed 2.5 wt% of H$_2$, which was almost the same capacity as that of the doped composite of MgH$_2$ + 10 wt% K$_2$NiF$_6$. By contrast, hydrogen absorbed by the MgH$_2$ + 10 wt% K$_2$NiF$_6$ + 5 wt% CNTs and MgH$_2$ + 10 wt% K$_2$NiF$_6$ + 10 wt% CNTs samples reached approximately 3.4 and 3.1 wt% of H$_2$, respectively, in the same time period. Therefore, the hydrogen absorption behaviour was affected by the amount of catalyst. These results indicated a synergetic catalytic effect from the combination of K$_2$NiF$_6$ and CNTs for MgH$_2$.

Fig. 2(b) displays the isothermal dehydrogenation kinetics curve for as-milled MgH$_2$, MgH$_2$ + 10 wt% K$_2$NiF$_6$, MgH$_2$ + 10 wt% K$_2$NiF$_6$ + 5 wt% CNTs, and the MgH$_2$ + 10 wt% K$_2$NiF$_6$ + 10 wt% CNTs composite, which were measured at 320 °C
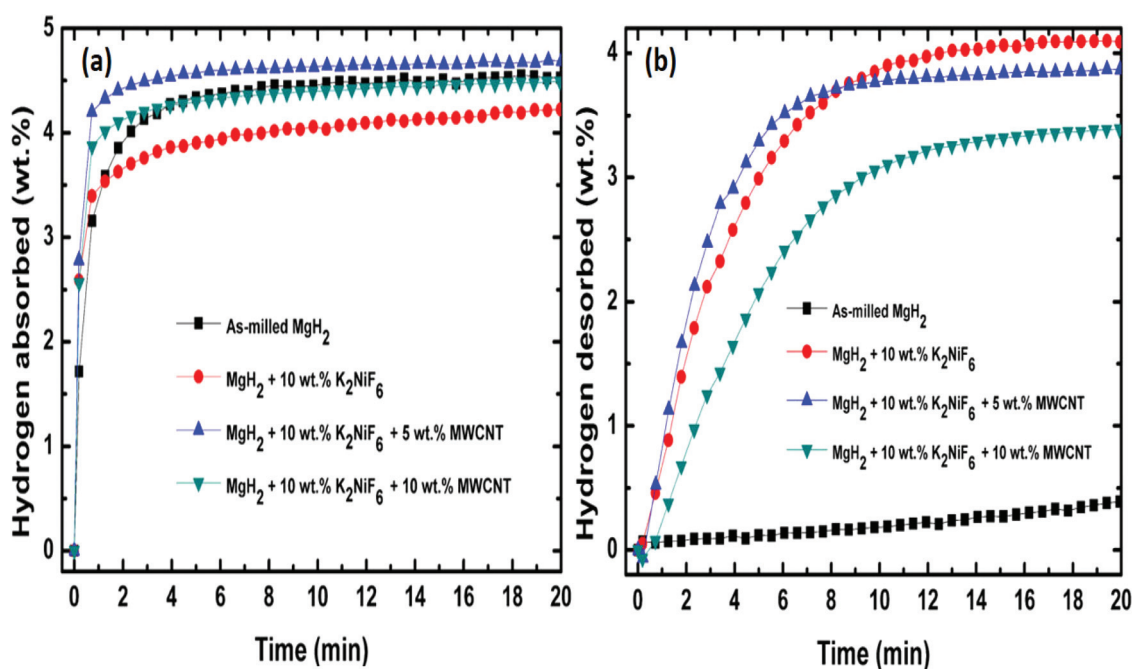

Fig. 2 Isothermal rehydrogenation kinetics curves at 320 °C and under 33.0 atm (a) and isothermal dehydrogenation kinetics at 320 °C and under 1.0 atm (b) of as-milled MgH$_2$, MgH$_2$ + 10 wt% K$_2$NiF$_6$, MgH$_2$ + 10 wt% K$_2$NiF$_6$ + 5 wt% CNTs and MgH$_2$ + 10 wt% K$_2$NiF$_6$ + 10 wt% CNTs.

and under 1.0 atm of H_2. Evidently, the doped samples displayed a great enhancement compared with the un-doped sample. The MgH_2 + 10 wt%K_2NiF_6 + 5 wt% CNTs and the MgH_2 + 10 wt% K_2NiF_6 + 10 wt% CNTs composites released 3.3 and 2.1 wt% hydrogen in 5 min after 1 h of dehydrogenation, respectively. The results displayed that the sample of MgH_2 + 10 wt% K_2NiF_6 + 5 wt% CNTs had faster hydrogen desorption kinetics than MgH_2 + 10 wt% K_2NiF_6 + 10 wt% CNTs. It can be concluded that the amount of catalyst can affect the hydrogen desorption behaviour. This finding can be supported with a study by Ranjbar et al.[37] They claimed that the kinetics results could be improved by the decrement of the grain size of MgH_2, but if too much catalyst is added to the sample it would obstruct the hydrogen diffusion by blocking the diffusion paths. Oelerich et al.[38] also showed that as little as 0.2 mol% of the catalyst was effective to present the fastest sorption kinetics. By contrast, MgH_2 doped with 10 wt% K_2NiF_6 released 3.0 wt% hydrogen, whereas almost no hydrogen (0.1 wt% hydrogen) was desorbed by using the as-milled MgH_2 sample in the same time period. Taken together, these results proposed that the enhancement of the dehydrogenation kinetics of the MgH_2–K_2NiF_6 composite was due to the addition of CNTs. The doping amount of 5 wt% CNTs could be considered the best compromise in terms of the dehydrogenation temperature and isothermal de/rehydrogenation kinetics compared with 10 wt% CNTs. Thus, identification of the optimal 5 wt% amount of CNTs led to the analysis of the MgH_2–K_2NiF_6–CNTs mechanism and the catalytic effect in subsequent tests.

The thermal properties of the as-received MgH_2, as-milled MgH_2, MgH_2 + 10 wt% K_2NiF_6, and MgH_2 + 10 wt% K_2NiF_6 + 5 wt% CNTs samples were further studied by DSC, as shown in Fig. 3. In the graph, the curve of the as-received MgH_2 displayed only one strong endothermic peak at approximately 484.20 °C, which corresponded to the decomposition of MgH_2.
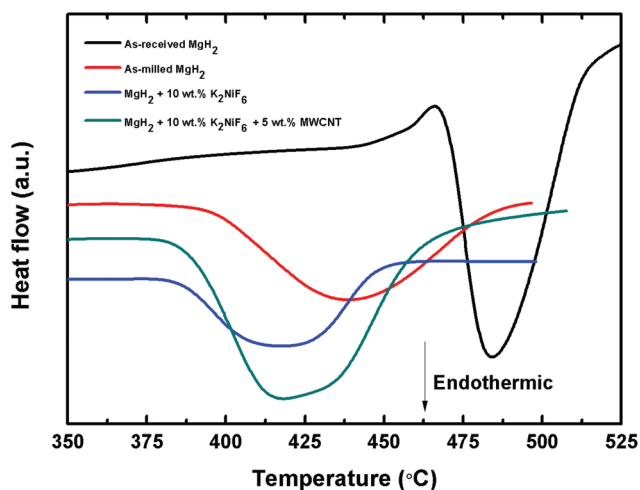

Fig. 3 DSC traces of the as-received MgH_2, as-milled MgH_2, MgH_2 + 10 wt% K_2NiF_6, and MgH_2 + 10 wt% K_2NiF_6 + 5 wt% CNTs (heating rate: 30 °C min⁻¹; argon flow: 50 ml min⁻¹).

The results from the DSC curves of the as-milled MgH_2, MgH_2 + 10 wt% K_2NiF_6 and MgH_2 + 10 wt% K_2NiF_6 + 5 wt% CNTs samples were similar to those of the as-received MgH_2 sample, showing only single endothermic peaks at 438.75 °C, 418.37 °C and 416.92 °C, respectively. The DSC results further indicated the synergetic effect of K_2NiF_6 and CNTs on the dehydrogenation of MgH_2, which was due to the notable decrement in the peak temperatures of the samples.

The Kissinger equation[39] shown below was used to calculate the apparent activation energy, E_a of the as-received MgH_2, as-milled MgH_2, MgH_2 + 10 wt% K_2NiF_6, and MgH_2 + 10 wt% K_2NiF_6 + 5 wt% CNTs at different heating rates. The Kissinger equation is stated below:

$$\ln[\beta/T_p^2] = -E_a/RT_p + A \qquad (1)$$

where β is the heating rate, T_p is the peak temperature in the DSC curve, R is the gas constant, and A is a linear constant. Thus, the activation energy, E_a, can be obtained from the slope in a plot of $\ln[\beta/T_p^2]$ versus $1000/T_p$. Fig. 4(a)–(d) display the DSC curves at different heating rates for all the samples studied. As shown in Fig. 5, from a Kissinger plot of the DSC data, the apparent activation energy, E_a, for the MgH_2 + 10 wt% K_2NiF_6 sample was found to be 100.0 kJ mol⁻¹, which was lower than that of as-received and as-milled MgH_2 (175.0 and 133.0 kJ mol⁻¹, respectively). After co-doping with K_2NiF_6 and CNTs, the activation energy was lowered to 70.0 kJ mol⁻¹, which displayed a great enhancement in kinetics by 30.0 kJ mol⁻¹ as compared with MgH_2 doped with K_2NiF_6. This result seems to be consistent with previous studies that found that the improvement in the dehydrogenation kinetics is due to the reduction in the activation energy after the addition of a catalyst.[16,40–42] In the present study, MgH_2 co-doped with K_2NiF_6 and CNTs reduced the activation energy for the decomposition of MgH_2 caused by ball milling and doping with a co-catalyst. These improvements in the decomposition properties were also related to the energy barrier for H_2 released from MgH_2. The results clearly showed the existence of synergistic catalysis between K_2NiF_6 and CNTs for MgH_2.

Fig. 6 presents the SEM images of the as-received MgH_2, as-received CNTs, as-milled MgH_2, MgH_2 + 10 wt% K_2NiF_6, and MgH_2 + 10 wt% K_2NiF_6 + 5 wt% CNTs. The particle size of the un-milled sample was larger than that of the milled sample after 1 h of ball milling. Fig. 6(a) displays the particle size of as-received MgH_2, and the sample was larger than 100 μm. The unique nanostructure of CNTs prior to ball milling is displayed in Fig. 6(b). The MgH_2 sample that encountered 1 h of ball milling exhibited a dramatic increase in the average size of MgH_2 particles, as shown in Fig. 6(c).

The particle size was not homogeneous and included some agglomerates, which were identified in the sample. Fig. 6(d) reveals that MgH_2 doped with 10 wt% K_2NiF_6 had the smallest particle size compared with the as-received and as-milled MgH_2. The small particle size increased the rate of reaction for MgH_2 because of the increase in the surface area of the sample. Zhang et al.[43] reported that large surface areas can be
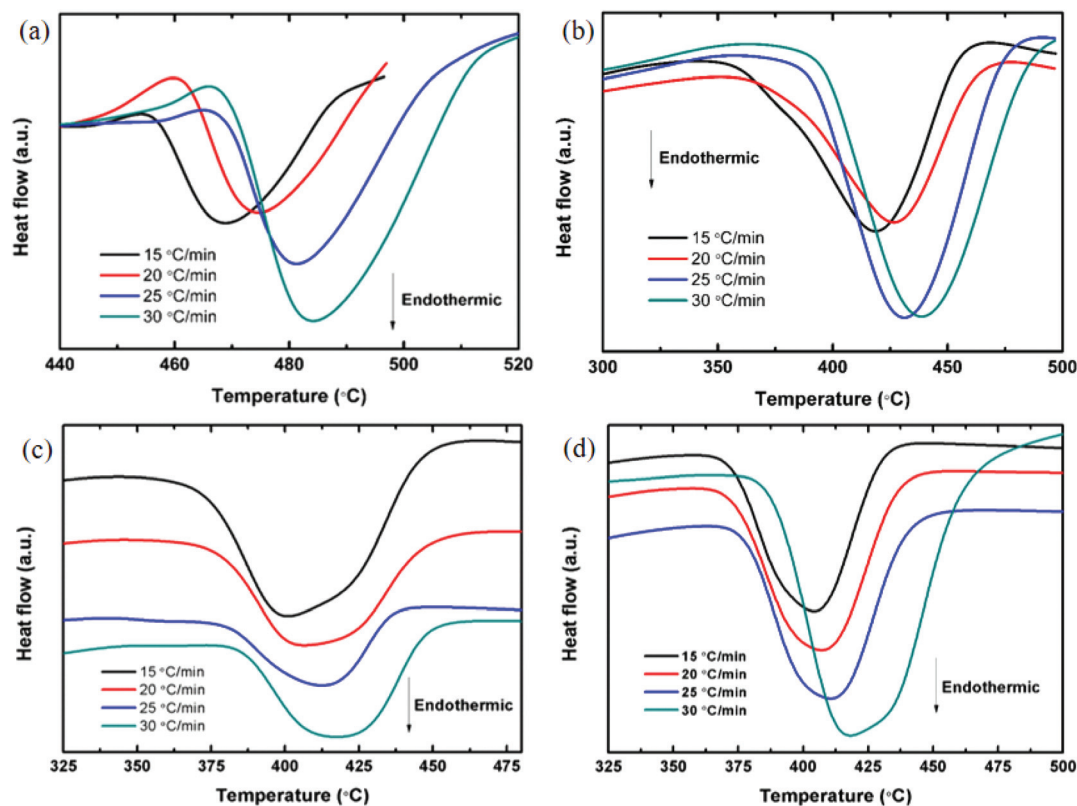
Fig. 4   DSC traces of (a) as-received MgH_2, (b) as-milled MgH_2, (c) MgH_2 + 10 wt% K_2NiF_6, and (d) MgH_2 + 10 wt% K_2NiF_6 + 5 wt% CNTs at different heating rates of 15–30 °C min^{-1}; argon flow: 50 ml min^{-1}.
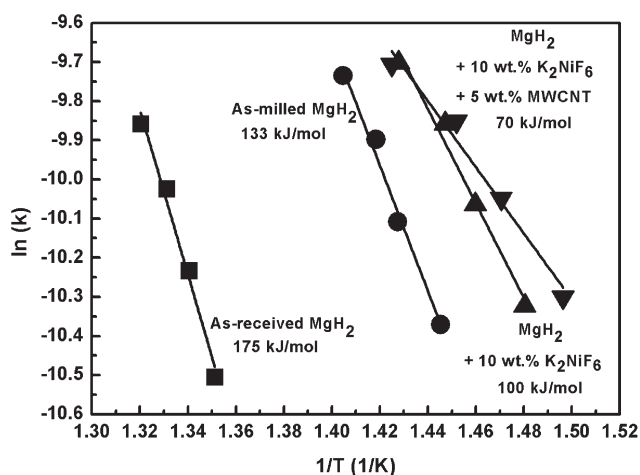
Fig. 5   Kissinger plot of as-received MgH_2, as-milled MgH_2, MgH_2 + 10 wt% K_2NiF_6, and MgH_2 + 10 wt% K_2NiF_6 + 5 wt% CNTs composite.

obtained from the nanostructured material, which led to the formation of more defects on the particle surfaces, heterogeneous nucleation of the product phase, shortening of the diffusion length of the constitutive elements and lowering of the hydrogen reaction enthalpy. The image also displays that the sample was irregularly shaped and agglomerated, which

showed the typical morphology of the ball-milled powders. Fig. 6(e) displays the SEM image of MgH_2 co-doped with 10 wt% K_2NiF_6 + 5 wt% CNTs. The addition of CNTs to the sample of MgH_2 + 10 wt% K_2NiF_6 could enhance the hydrogen storage properties of MgH_2 because of the lower particle agglomeration. However, the difference of particle agglomeration between the MgH_2 + 10 wt% K_2NiF_6, and MgH_2 + 10 wt% K_2NiF_6 + 5 wt% CNTs samples was not really obvious. After 1 h of ball milling, the CNTs were not destroyed, which correlated with the findings of previous studies.[31,44] Wu et al.[45] also claimed that the special microstructure of CNTs may facilitate the desorption of hydrogen from $Zn(BH_4)_2$ even though CNTs may be shortened or partly destroyed during ball milling. Moreover, the sample that was co-doped with K_2NiF_6 and CNTs also appeared to exhibit less agglomeration.

To clarify the reaction progress and phase structures of the MgH_2 + 10 wt% K_2NiF_6 + 5 wt% CNTs samples, XRD measurements were performed on the samples after 1 h of ball milling, after dehydrogenation at 450 °C and after rehydrogenation at 320 °C and under 33.0 atm hydrogen pressure (Fig. 7). As shown in Fig. 7(a), only a single MgH_2 peak dominated the XRD pattern after 1 h of milling. However, the K_2NiF_6-containing phase or CNTs could not be detected after milling, which was probably due to the low amount of K_2NiF_6 and CNTs as detected by XRD. This finding may also be due to the peaks of K_2NiF_6 and CNTs that transformed into an
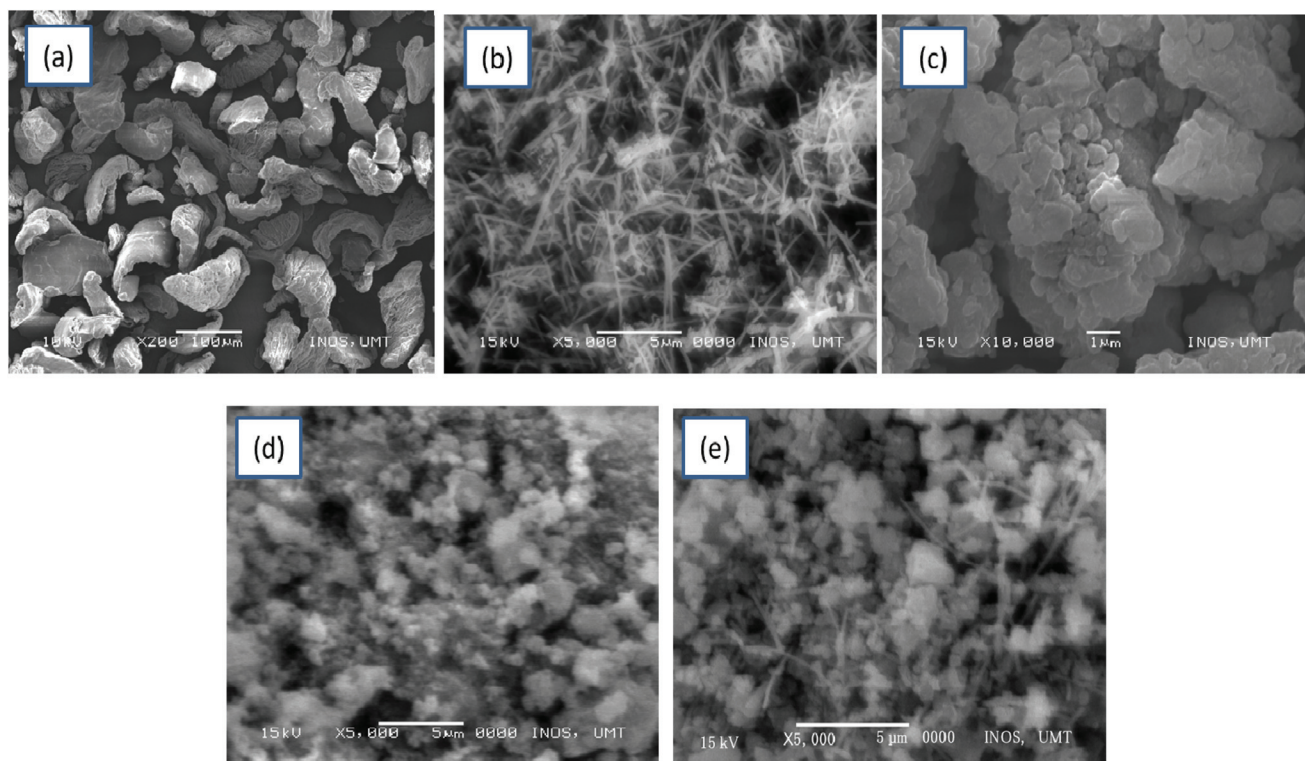
Fig. 6 The SEM images of the (a) as-received MgH_2, (b) as-received CNTs, (c) as-milled MgH_2, (d) MgH_2 + 10 wt% K_2NiF_6 and (e) MgH_2 + 10 wt% K_2NiF_6 + 5 wt% CNTs.
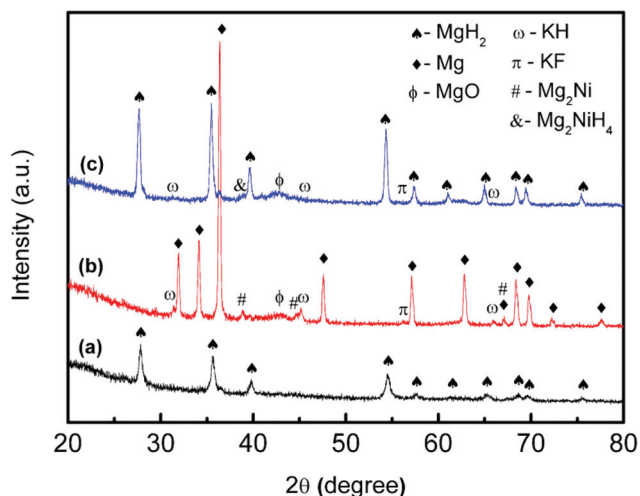
Fig. 7 XRD patterns of MgH_2 + 10 wt% K_2NiF_6 + 5 wt% CNTs (a) after ball milling for 1 h, (b) after dehydrogenation at 450 °C and (c) after rehydrogenation at 320 °C.

amorphous state directly after ball milling. After heating to 450 °C, MgH_2 from the as-milled pattern disappeared and fully transformed into Mg, which showed that the dehydrogenation process of MgH_2 was completed (Fig. 7(b)). Meanwhile, a small MgO peak was detected after dehydrogenation; this peak possibly resulted from the low oxygen contamination when transfer-

ring the samples to the XRD instrument. Moreover, some peaks of KF, KH and Mg_2Ni were also observed after dehydrogenation, thereby proposing that several reactions occurred during dehydrogenation between MgH_2 and K_2NiF_6. The rehydrogenation of MgH_2 co-doped with K_2NiF_6 and CNTs at 320 °C (Fig. 7(c)) represented the major peaks of MgH_2. In addition, MgO could still be detected in the XRD spectra, together with the peaks of KF and KH that remained unchanged after rehydrogenation. The new peak of Mg_2NiH_4 that formed because of the absorption of hydrogen by Mg_2Ni was also detected. The formation of Mg_2NiH_4 can be represented in the following equation:

$$Mg_2Ni + 2H_2 \rightarrow Mg_2NiH_4. \qquad (2)$$

As no CNTs peak was detected in the phase composition of the sample with 5 wt% CNTs, the sample with 10 wt% CNTs was prepared for XRD to study the phase structure. Fig. 8 shows the XRD patterns of MgH_2 + 10 wt% K_2NiF_6 + 10 wt% CNTs after 1 h of ball milling, after dehydrogenation at 450 °C and after rehydrogenation at 320 °C and under hydrogen pressure of 33.0 atm. After increasing the amount of CNTs to 10 wt%, the peak of CNTs after ball milling was noted in the XRD spectra (Fig. 8(a)). The peak of MgH_2 still dominated the XRD pattern after 1 h of milling. The spectra of dehydrogenated samples (Fig. 8(b)) represented the major peaks of Mg, and the peak of CNTs was still present. In addition, the same new species of KH, KF and Mg_2Ni peaks were noted.
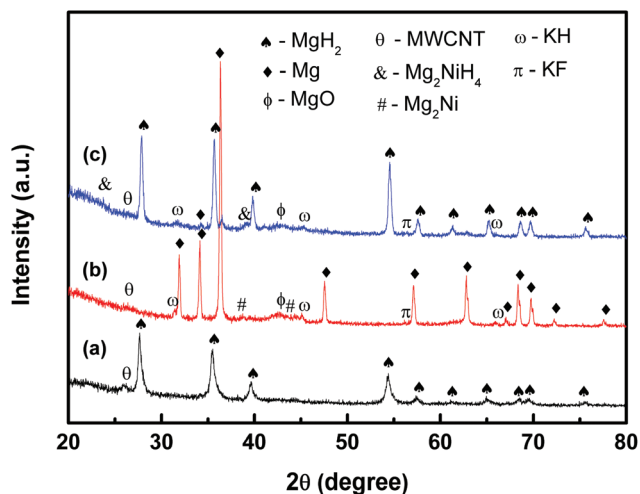
Fig. 8 XRD patterns of MgH_2 + 10 wt% K_2NiF_6 + 10 wt% CNTs (a) after ball milling for 1 h, (b) after dehydrogenation at 450 °C and (c) after rehydrogenation at 320 °C.

and reduces the reaction temperature.[60] Mao *et al.*[61] also claimed that Mg_2Ni is more active than Mg_2CO, because of the improvement of dehydrogenation of MgH_2 doped with $MgCl_2$ and Mg_2Ni compared with MgH_2 doped with $MgCl_2$ and Mg_2CO.

The catalytic effect of CNTs may also play an important role in improving the hydrogen storage properties of the MgH_2/K_2NiF_6/CNTs composite. Previous studies have shown that the unique nanostructure of CNTs is expected to form a net-like architecture after being milled together with the host materials and acting as a diffusion channel for hydrogen.[62,63] In addition, the enhancement of the CNTs-added MgH_2–K_2NiF_6 sample may also have been due to the hardness of CNTs. The presence of CNTs in the MgH_2–K_2NiF_6 composite prevented particle agglomeration, as shown in Fig. 6(e). The hydrogen storage properties of light metal hydrides improved with reduced particle agglomeration.[64] Hence, the enhanced hydrogenation process of MgH_2 co-doped with K_2NiF_6 and CNTs was due to the combination of the *in situ* active species of KF, KH and Mg_2Ni with the catalytic effect of CNTs.

A small amount of MgO was also detected in the peak that resulted from minimal oxygen contamination. Meanwhile, the XRD patterns of the rehydrogenated sample showed that Mg had largely transformed into MgH_2 (Fig. 8(c)). However, some peaks of Mg could be observed in the XRD patterns, which possibly resulted from the Mg that was not fully reversible in the process. Meanwhile, the peaks of MgO and CNTs could still be detected, along with the peaks of species KH and KF that remained unchanged after rehydrogenation. The peaks of Mg_2NiH_4 were also detected in the pattern.

The results of this study indicated that the formation of *in situ* active species KF, KH and Mg_2Ni, which resulted from the reaction of MgH_2 and K_2NiF_6 during dehydrogenation, may play an important role in the improvement of MgH_2 sorption. Recent studies revealed that the decrement of the dehydrogenation temperature of metal hydrides and complex hydrides is due to the catalytic effects of the F^- anion.[46–49] Wang *et al.*[50] also reported the optimal performance of TiF_3 over $TiCl_3$. Liu *et al.*[49] conducted structural analyses and found that the F^- anions can partially substitute the H^- anions in the hydride lattice, thereby weakening the Al–H bonds and reducing the thermodynamic stability. In addition, a previous study on the Mg based composite revealed that the catalyst helps to dissociate the hydrogen molecule to enhance the absorption and desorption rate together with the decrement of the desorption temperature.[51–53]

Numerous studies verified that significant improvements of metal hydride/complex hydride sorption properties are attributed to the synergistic effects of *in situ* formed hydride species *via* the decomposition of host materials.[54,55] For example, Xiao *et al.*[56] revealed that the dehydrogenation properties of the second step reaction of the $NaAlH_4$ system can be enhanced by the addition of KH. Moreover, the addition of KH can significantly enhance the dehydrogenation properties of $NaAlH_4$ and $Mg(NH_2)_2$/2LiH systems.[57–59] Mg_2Ni has also been reported as an effective catalyst that increases the reaction rates of MgH_2

4. Conclusion

The hydrogen storage properties of MgH_2 improved after doping with K_2NiF_6 and CNTs. The addition of K_2NiF_6 co-catalyzed with CNTs reduced the dehydrogenation temperature and improved the de/rehydrogenation kinetics of MgH_2 compared with the MgH_2–K_2NiF_6 composite. The MgH_2 + 10 wt% K_2NiF_6 + 5 wt% CNTs sample started to release hydrogen at around 245 °C with a total dehydrogenation capacity of 5.1 wt%, decreased by approximately 25 °C compared with MgH_2 + 10 wt% K_2NiF_6. In terms of rehydrogenation kinetics, MgH_2 co-doped with 10 wt% K_2NiF_6 and 5 wt% CNTs samples absorbed 3.4 wt% of hydrogen in 1 min at 320 °C and under 33.0 atm of hydrogen, whereas the MgH_2 + 10 wt% K_2NiF_6 sample absorbed 2.6 wt% of hydrogen under the same conditions. For the dehydrogenation kinetics under 1.0 atm of hydrogen and 320 °C, the MgH_2 + 10 wt% K_2NiF_6 + 5 wt% CNTs sample released 3.3 wt% hydrogen after 5 min of dehydrogenation. By contrast, MgH_2 doped with 10 wt% K_2NiF_6 released 3.0 wt% hydrogen in the same time period. The results from the Kissinger plot displayed that the apparent activation energy, E_a, for MgH_2 co-doped with K_2NiF_6 and CNTs was lowered to 70.0 kJ mol^{-1}, which showed a great enhancement in kinetics by 30.0 kJ mol^{-1} as compared with MgH_2 doped with 10 wt% K_2NiF_6 (E_a = 100.0 kJ mol^{-1}). It is believed that the newly developed product of KF, KH and Mg_2Ni together with the unique structure of the CNTs functioned as a real catalyst and then generated a synergetic effect to enhance the hydrogen storage properties of MgH_2.

Acknowledgements

References

1 I. P. Jain, C. Lal and A. Jain, *Int. J. Hydrogen Energy*, 2010, **35**, 5133–5144.

2 M. Ismail, Y. Zhao, X. B. Yu and S. X. Dou, *RSC Adv.*, 2011, **1**, 408–414.

3 S. Srinivasa Murthy and E. Anil Kumar, *Appl. Therm. Eng.*, 2014, **72**, 176–189.

4 X. Wu, R. Zhang and J. Yang, *Phys. Chem. Chem. Phys.*, 2016, **18**, 19412–19419.

5 J. Huot, G. Liang, S. Boily, A. Van Neste and R. Schulz, *J. Alloys Compd.*, 1999, **293–295**, 495–500.

6 M. Ismail, Y. Zhao, X. B. Yu and S. X. Dou, *Int. J. Hydrogen Energy*, 2012, **37**, 8395–8401.

7 L. Z. Ouyang, X. S. Yang, M. Zhu, J. W. Liu, H. W. Dong, D. L. Sun, J. Zou and X. D. Yao, *J. Phys. Chem. C*, 2014, **118**, 7808–7820.

8 N. N. Sulaiman, N. S. Mustafa and M. Ismail, *Dalton Trans.*, 2016, **45**, 7085–7093.

9 X. Xiao, Z. Liu, S. Saremi-Yarahmadi and D. H. Gregory, *Phys. Chem. Chem. Phys.*, 2016, **18**, 10492–10498.

10 Y. Zhang, Q.-F. Tian, S.-S. Liu and L.-X. Sun, *J. Power Sources*, 2008, **185**, 1514–1518.

11 L. Z. Ouyang, Z. J. Cao, H. Wang, J. W. Liu, D. L. Sun, Q. A. Zhang and M. Zhu, *J. Alloys Compd.*, 2014, **586**, 113–117.

12 L. Ouyang, Z. Cao, H. Wang, R. Hu and M. Zhu, *J. Alloys Compd.*, 2017, **691**, 422–435.

13 L. Z. Ouyang, S. Y. Ye, H. W. Dong and M. Zhu, *Appl. Phys. Lett.*, 2007, **90**, 021917.

14 L. Z. Ouyang, Z. J. Cao, L. L. Li, H. Wang, J. W. Liu, D. Min, Y. W. Chen, F. M. Xiao, R. H. Tang and M. Zhu, *Int. J. Hydrogen Energy*, 2014, **39**, 12765–12772.

15 L. Z. Ouyang, Z. J. Cao, H. Wang, J. W. Liu, D. L. Sun, Q. A. Zhang and M. Zhu, *Int. J. Hydrogen Energy*, 2013, **38**, 8881–8887.

16 Z. Cao, L. Ouyang, Y. Wu, H. Wang, J. Liu, F. Fang, D. Sun, Q. Zhang and M. Zhu, *J. Alloys Compd.*, 2015, **623**, 354–358.

17 G. Liang, J. Huot, S. Boily, A. Van Neste and R. Schulz, *J. Alloys Compd.*, 1999, **292**, 247–252.

18 X. B. Yu, Z. X. Yang, H. K. Liu, D. M. Grant and G. S. Walker, *Int. J. Hydrogen Energy*, 2010, **35**, 6338–6344.

19 M. Ismail, *Energy*, 2015, **79**, 177–182.

20 I. E. Malka, T. Czujko and J. Bystrzycki, *Int. J. Hydrogen Energy*, 2010, **35**, 1706–1712.

21 L. P. Ma, X. D. Kang, H. B. Dai, Y. Liang, Z. Z. Fang, P. J. Wang, P. Wang and H. M. Cheng, *Acta Mater.*, 2009, **57**, 2250–2258.

22 M. Ismail, *Int. J. Hydrogen Energy*, 2014, **39**, 2567–2574.

23 M. A. Lillo-Ródenas, Z. X. Guo, K. F. Aguey-Zinsou, D. Cazorla-Amorós and A. Linares-Solano, *Carbon*, 2008, **46**, 126–137.

24 A. Kubota, H. Miyaoka, M. Tsubota, K. Shimoda, T. Ichikawa and Y. Kojima, *Carbon*, 2013, **56**, 50–55.

25 B. S. Amirkhiz, M. Danaie, M. Barnes, B. Simard and D. Mitlin, *J. Phys. Chem. C*, 2010, **114**, 3265–3275.

26 C. Z. Wu, P. Wang, X. Yao, C. Liu, D. M. Chen, G. Q. Lu and H. M. Cheng, *J. Alloys Compd.*, 2006, **420**, 278–282.

27 Y. Luo, P. Wang, L.-P. Ma and H.-M. Cheng, *Scr. Mater.*, 2007, **56**, 765–768.

28 X. Yao, C. Wu, A. Du, J. Zou, Z. Zhu, P. Wang, H. Cheng, S. Smith and G. Lu, *J. Am. Chem. Soc.*, 2007, **129**, 15650–15654.

29 B. S. Amirkhiz, M. Danaie and D. Mitlin, *Nanotechnology*, 2009, **20**, 204016.

30 C. Wu, P. Wang, X. Yao, C. Liu, D. Chen, G. Q. Lu and H. Cheng, *J. Phys. Chem. B*, 2005, **109**, 22217–22221.

31 M. Ismail, N. Juahir and N. S. Mustafa, *J. Phys. Chem. C*, 2014, **118**, 18878–18883.

32 A. Ranjbar, M. Ismail, Z. P. Guo, X. B. Yu and H. K. Liu, *Int. J. Hydrogen Energy*, 2010, **35**, 7821–7826.

33 M. G. Verón, H. Troiani and F. C. Gennari, *Carbon*, 2011, **49**, 2413–2423.

34 N. N. Sulaiman, N. Juahir, N. S. Mustafa, F. A. Halim Yap and M. Ismail, *J. Energy Chem.*, 2016, **25**, 832–839.

35 F. A. Halim Yap, N. S. Mustafa and M. Ismail, *RSC Adv.*, 2015, **5**, 9255–9260.

36 G. Barkhordarian, T. Klassen and R. Bormann, *J. Alloys Compd.*, 2004, **364**, 242–246.

37 A. Ranjbar, Z. P. Guo, X. B. Yu, D. Wexler, A. Calka, C. J. Kim and H. K. Liu, *Mater. Chem. Phys.*, 2009, **114**, 168–172.

38 W. Oelerich, T. Klassen and R. Bormann, *J. Alloys Compd.*, 2001, **322**, L5–L9.

39 H. E. Kissinger, *Anal. Chem.*, 1957, **29**, 1702–1706.

40 L. Z. Ouyang, X. S. Yang, H. W. Dong and M. Zhu, *Scr. Mater.*, 2009, **61**, 339–342.

41 M. Ma, R. Duan, L. Ouyang, X. Zhu, Z. Chen, C. Peng and M. Zhu, *J. Alloys Compd.*, 2017, **691**, 929–935.

42 D. Wu, L. Ouyang, C. Wu, Q. Gu, H. Wang, J. Liu and M. Zhu, *J. Alloys Compd.*, 2017, **690**, 519–522.

43 Z. Zhang, S. Zhang, H. Wang, J. Liu and M. Zhu, *J. Alloys Compd.*, 2010, **505**, 717–721.

44 A. Kukovecz, T. Kanyo, Z. Konya and I. Kiricsi, *Carbon*, 2005, **43**, 994–1000.

45 C. Wu, P. Wang, X. Yao, C. Liu, D. Chen, G. Lu and H. Cheng, *J. Alloys Compd.*, 2006, **414**, 259–264.

46 L.-P. Ma, P. Wang and H.-M. Cheng, *Int. J. Hydrogen Energy*, 2010, **35**, 3046–3050.

47 L.-C. Yin, P. Wang, X.-D. Kang, C.-H. Sun and H.-M. Cheng, *Phys. Chem. Chem. Phys.*, 2007, **9**, 1499–1502.

48 H. W. Brinks, A. Fossdal and B. C. Hauback, *J. Phys. Chem. C*, 2008, **112**, 5658–5661.

49 Y. Liu, F. Wang, Y. Cao, M. Gao, H. Pan and Q. Wang, *Energy Environ. Sci.*, 2010, **3**, 645–653.

50 P. Wang, X. D. Kang and H. M. Cheng, *ChemPhysChem*, 2005, **6**, 2488–2491.

51 L. Xie, Y. Liu, Y. T. Wang, J. Zheng and X. G. Li, *Acta Mater.*, 2007, **55**, 4585–4591.

52 L. Z. Ouyang, H. Wang, M. Zhu, J. Zou and C. Y. Chung, *Microsc. Res. Tech.*, 2004, **64**, 323–329.

53 L. Ouyang, J. Tang, Y. Zhao, H. Wang, X. Yao, J. Liu, J. Zou and M. Zhu, *Sci. Rep.*, 2015, **5**, 10776.

54 Y. Li, F. Fang, Y. Song, Y. Li, D. Sun, S. Zheng, L. A. Bendersky, Q. Zhang, L. Ouyang and M. Zhu, *Dalton Trans.*, 2013, **42**, 1810–1819.

55 J. Huang, Y. Yan, L. Ouyang, H. Wang, J. Liu and M. Zhu, *Dalton Trans.*, 2014, **43**, 410–413.

56 X. Xiao, S. Wang, X. Fan, C. Xu, J. Sun, Q. Wang and L. Chen, *Int. J. Hydrogen Energy*, 2014, **39**, 6577–6587.

57 Y. Liu, C. Liang, H. Zhou, M. Gao, H. Pan and Q. Wang, *Chem. Commun.*, 2011, **47**, 1740–1742.

58 J. Wang, T. Liu, G. Wu, W. Li, Y. Liu, C. M. Araújo, R. H. Scheicher, A. Blomqvist, R. Ahuja, Z. Xiong, P. Yang, M. Gao, H. Pan and P. Chen, *Angew. Chem., Int. Ed.*, 2009, **48**, 5828–5832.

59 P. Wang, X. D. Kang and H. M. Cheng, *J. Appl. Phys.*, 2005, **98**, 5.

60 S. T. Sabitu, G. Gallo and A. J. Goudy, *J. Alloys Compd.*, 2010, **499**, 35–38.

61 J. Mao, Z. Guo, X. Yu, H. Liu, Z. Wu and J. Ni, *Int. J. Hydrogen Energy*, 2010, **35**, 4569–4575.

62 M. Ismail, Y. Zhao, X. B. Yu, A. Ranjbar and S. X. Dou, *Int. J. Hydrogen Energy*, 2011, **36**, 3593–3599.

63 Z. Z. Fang, X. D. Kang, H. B. Dai, M. J. Zhang, P. Wang and H. M. Cheng, *Scr. Mater.*, 2008, **58**, 922–925.

64 P. Adelhelm and P. E. de Jongh, *J. Mater. Chem.*, 2011, **21**, 2417–2427.